Monte Carlo Study of the Formation and Conformational Properties of Dimers of Aβ42 Variants

Simon Mitternacht[1,2,†], Iskra Staneva[1,†], Torleif Härd[3] and Anders Irbäck[1,*]

[1]Computational Biology & Biological Physics, Lund University, Sölvegatan 14A, SE-223 62 Lund, Sweden. [2]Department of Informatics, University of Bergen, PB 7803, N-5020 Bergen, Norway. [3]Department of Molecular Biology, Swedish University of Agricultural Sciences (SLU), Box 590, SE-751 24 Uppsala, Sweden

[†] S.M. and I.S. contributed equally to this work.

[*] Corresponding author. Phone: +46-46-2223493. Fax: +46-46-2229686. Email: anders@thep.lu.se.

Small soluble oligomers, and dimers in particular, of the amyloid β-peptide (Aβ) are believed to play an important pathological role in Alzheimer's disease (AD). Here we investigate the spontaneous dimerization of Aβ42, with 42 residues, by implicit solvent all-atom Monte Carlo (MC) simulations, for the wild type (WT) peptide and the mutants F20E, E22G and E22G/I31E. The observed dimers of these variants share many overall conformational characteristics, but differ in several aspects at a detailed level. In all four cases, the most common type of secondary structure is intramolecular antiparallel β-sheets. Parallel in-register β-sheet structure, as in models for Aβ fibrils, is rare. The primary force driving the formation of dimers is hydrophobic attraction. The conformational differences that we do see involve turns centered in the 20–30 region. The probability of finding turns centered in the 25–30 region, where there is a loop in Aβ fibrils, is found to increase upon dimerization and correlate with experimentally measured rates of fibril formation for the different Aβ42 variants. Our findings hint at reorganization of this part of the molecule as a potentially critical step in Aβ aggregation.

Keywords: amyloid; protein aggregation; oligomerization; molecular simulation; all-atom

Abbreviations: Aβ, amyloid β-peptide; AD, Alzheimer's disease; CHC, central hydrophobic cluster; MC, Monte Carlo

Introduction

Increasing evidence indicates that the primary pathogenic form of Aβ, the fibril-forming main component of amyloid plaques in AD, is small soluble oligomers, rather than mature fibrils [1]. In support of this hypothesis, it was demonstrated that Aβ dimers extracted from AD brain samples impair synapse structure and function in rats [2]. Further, it has been found that a familial AD-linked deletion mutant of Aβ (E22Δ) forms small oligomers, but very little fibrils [3]. Aβ oligomers of a double-cysteine mutant, called Aβ42CC, were, moreover, shown to be very potent inducers of neuronal apoptosis [4].

Over the past decade, atomic-level structural models of Aβ fibrils have been developed [5, 6]. In these models, each Aβ molecule participates in two intermolecular face-to-face packed β-sheets, both with a parallel, in-register organization. The two strand regions are connected by a loop at residues ∼25–30 to a β-loop-β motif. This overall fibril organization is shared by the WT variants of both Aβ40 [5] and Aβ42 [6], which are the two main isoforms of Aβ. By contrast, the Iowa mutant Aβ40 D23N was recently found to form fibrils with antiparallel β-sheets [7].

Less is known about the structure of Aβ oligomers, but several groups have recently reported successful studies of Aβ oligomers formed under different conditions, including tetramers [8], pentamers [9] as well as larger species [10]. These studies show, in particular, that the secondary structure of Aβ oligomers is generally different than that found in Aβ fibrils. In two of the studies, antiparallel β-sheets were observed [8, 10].

In this article, we investigate the elementary step of Aβ aggregation, the formation of dimers, by implicit solvent all-atom MC methods. We focus on Aβ42, with 42 residues, which is the form of Aβ most closely linked to AD. Starting from random initial conformations, we study the ensembles of dimeric states populated by Aβ42 WT and the three mutants E22G, E22G/I31E and F20E. These Aβ42 variants are deliberately chosen to have very different in vitro aggregation properties, and have been found to differ also in terms of their effects on the fitness of transgenic fruit flies [11]. The E22G mutation, which is associated with the familial so-called Arctic form of AD [12], is known to enhance aggregation, whereas the F20E mutation has the reverse effect [11]. The double mutant E22G/I31E shows more complex aggregation properties. Its propensity to form fibrils is almost as high as that of the E22G variant, whereas its propensity to form prefibrillar species is only slightly higher than that of the F20E variant [11, 13].

In previous computational studies of Aβ dimers, one approach has been to examine the stability of preformed structures [14, 15]. Also, a first study of spontaneous dimer formation was

reported [16]. However, simulating the spontaneous dimerization of full-length Aβ molecules is a challenge. Here we tackle this problem by using MC techniques and an effective force field (see Methods). This force field was developed through folding thermodynamics studies of a structurally diverse set of peptides and small proteins, while deliberately keeping it as simple as possible [17].

Based on the same computational model, we recently investigated [18] the natively unfolded Aβ42 monomer [19–21]. To validate the simulations, we compared calculated NMR properties (J-couplings and chemical shifts) with experimental data (see Methods). We found that the Aβ42 monomer populates a multitude of β-sheet containing states, and further observed small but clear conformational effects of the E22G, E22G/I31E and F20E mutations.

Results

Using simulated tempering MC techniques and an effective implicit solvent all-atom potential, we study the conformational ensemble populated by two Aβ42 peptides enclosed in a cubic box, under periodic boundary and random initial conditions (see Methods). The simulation temperatures are between T_0 and $\sim$1.2 T_0, where T_0 denotes the temperature used in our previous monomer study and corresponds to $\sim$273–278 K in physical units [18]. Our present study focuses primarily on properties at the same temperature T_0, but we begin with a brief discussion of how the state of aggregation of the systems (WT, F20E, E22G, E22G/I31E) depends on the simulation temperature.

Coalescence and ordering. The propensity of the peptides to interact and aggregate can be controlled by varying the simulation temperature; all four variants form bound dimeric states at T_0, while being unbound and disordered at $\sim$1.2 T_0. To examine the character of the transition between the monomer and dimer phases, we construct equilibrium free-energy surfaces at different temperatures. The properties monitored are the β-strand content, β, the radius of gyration of individual peptides, R_g, and the center-of-mass distance between the peptides, D_{cm}. The α-helix content is low (a few percent or lower) at all temperatures studied, and therefore not included in the analysis. Figure 1 shows the free energies $F(D_{cm}, R_g)$ and $F(D_{cm}, \beta)$ for WT, at the temperatures T_0 and 1.09 T_0. The latter temperature belongs to the transition region where the monomer (high D_{cm}) and dimer (small D_{cm}) phases coexist. At 1.09 T_0, the monomer and dimer populations are 0.60 and 0.40, respectively. The two coexisting phases are both conformationally heterogeneous, spanning broad (and overlapping) ranges in R_g and β. For the dimer ensemble, the average R_g

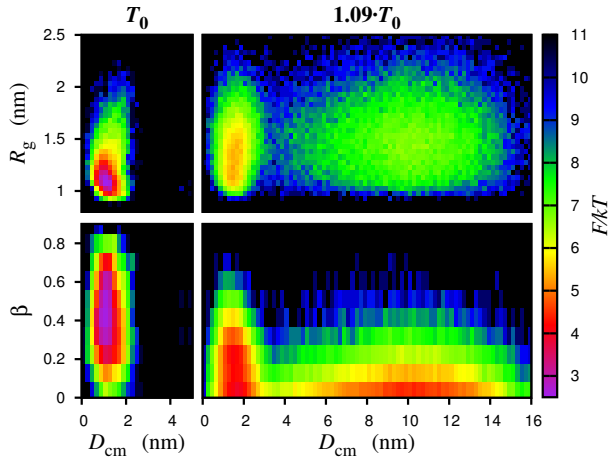

Figure 1: Free energies of binding for Aβ42 WT. The functions $F(D_{\mathrm{cm}}, R_{\mathrm{g}})$ and $F(D_{\mathrm{cm}}, \beta)$ at T_0, where dimeric states dominate, and at 1.09 T_0, where the dimer and monomer phases coexist.

and β values are 1.43 nm and 0.17, respectively. The corresponding values for the monomer ensemble are 1.54 nm and 0.10. Statistically, dimer formation thus induces increased compactness and order of the peptides. Both compactness and order increase further as the temperature is reduced to T_0, where dimeric states dominate completely (Fig. 1); at T_0, the average R_{g} and β values are 1.15 nm and 0.43, respectively. The differences in R_{g} and β between dimers observed at these two temperatures, T_0 and 1.09 T_0, are thus larger than the changes ensuing from dimerization, at 1.09 T_0.

The corresponding free energy diagrams for E22G and E22G/I31E (Supplementary Figs. S1 and S2) are very similar to those for WT shown in Fig. 1. The remaining F20E variant shows, by contrast, a different behavior. A main difference is that aggregation sets in at a lower temperature for F20E, which thus is less prone to aggregate. In fact, to have a dimer population comparable to that of WT at 1.09 T_0 (0.40), the temperature must be reduced to ∼1.04 T_0 for F20E (dimer population 0.32 at 1.04 T_0).

Figure 2 shows the free energies $F(D_{\mathrm{cm}}, R_{\mathrm{g}})$ and $F(D_{\mathrm{cm}}, \beta)$ for F20E at T_0 and at the coexistence temperature 1.04 T_0. At 1.04 T_0, the monomer and dimer ensembles have average β values of 0.18 and 0.36, respectively, while the average R_{g} is 1.47 nm for monomers and 1.35 nm for dimers. The change in β upon dimerization is large for this variant, and indicates that dimer formation is more cooperative than it is for the other three variants. This jump in β, in particular, means that disordered dimers with a low strand content are rare for F20E (see Fig. 2). The other three variants

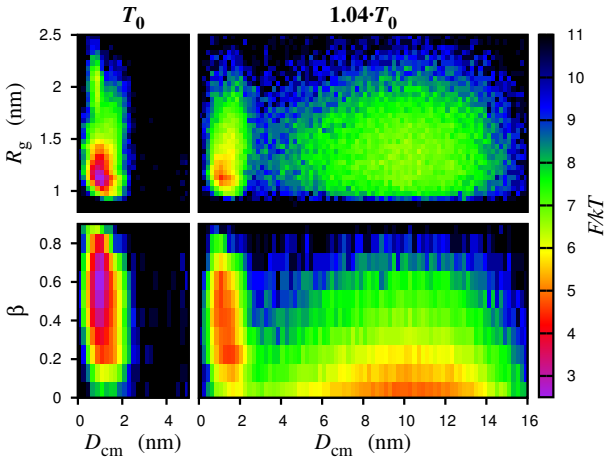

Figure 2: Free energies of binding for Aβ42 F20E. The functions $F(D_{cm}, R_g)$ and $F(D_{cm}, \beta)$ at T_0 and 1.04 T_0.

do form disordered dimers at their coexistence temperature (Figs. 1 and Supplementary Figs. S1 and S2).

We now turn to more detailed properties of the observed dimers. Throughout the rest of the paper, unless otherwise stated, we focus on results obtained at the temperature T_0.

Intramolecular contacts. To statistically describe the 3D organization of the dimers, we construct intra- and inter-chain contact maps. The probability of finding specific residue contacts within and between chains, at T_0, can be seen in Fig. 3. Except in the vicinity of the mutation sites, the contact maps are very similar for all four variants. This agreement between completely independent simulations makes us confident that the main features of the calculated contact maps are statistically robust.

We first discuss the intra-chain contact maps. Many of the observed intra-chain contacts can be associated with turns, recognized as bands extending perpendicularly from the diagonal.

One such band involves residues 10–19. Inspection shows that this band corresponds to a β-hairpin centered at residues 14 and 15. This hairpin contains four characteristic H bonds (connecting residues 11 and 18 and residues 13 and 16). The probability that a given peptide has at least three of these four H bonds present varies between 74–82 %, depending on Aβ42 variant. Hence, for all four variants, both peptides have this hairpin in the majority of the simulated conformations. In our previous monomer simulations [18], the hairpin population varied between 36–58 %, which is significantly lower compared to the dimer values. We thus find that dimer formation has a stabilizing effect on this hairpin.

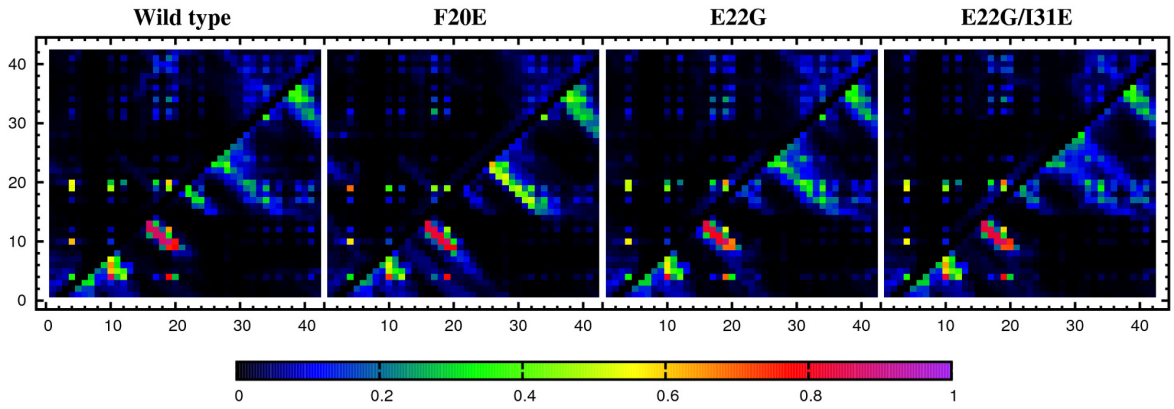

Figure 3: Probability maps of residue contact formation within and between chains. Intra- and inter-chain pair contact probabilities are shown below and above the main diagonal, respectively. Data are taken at T_0.

Of particular interest among the turns seen in Fig. 3 are those centered in the 20–30 region, partly because the loop region of Aβ42 fibrils is at residues ∼25–30 [6, 22, 23], but also because the mutations studied have clear effects on these turns. Other turns, like the 10–19 hairpin, are only weakly affected by the mutations.

For WT, we observe a small turn centered at residues 20 and 21 and a large one centered at residues 25 and 26. The main effect of the mutations on the small turn is to reduce its population; its shape is left essentially unaltered. The mutations cause, by contrast, changes in both location and character of the large turn. The F20E mutation makes this turn more narrow and shifts the statistically preferred center of the turn toward the N terminus, to residues 24 and 25. The E22G and E22G/I31E mutations lead instead to a broadening of the band of populated contacts, in the opposite direction, toward the C terminus. These observations indicate that the mutations, in particular, might affect the propensity of Aβ42 to form turns centered in the loop region 25–30 of fibrils.

To examine this effect quantitatively, we introduce a simple measure of the probability of observing turns centered in this region, n_{perp}. Specifically, we define n_{perp} as the sum of all intra-chain contact probabilities within a strip that perpendicularly intersects the main diagonal at residues 25–30. For comparison, we compute n_{perp} for the monomers as well, using data from our previous study [18]. Figure 4 presents the results of this analysis, which show that the three mutations indeed cause significant conformational changes in this part of the molecule. Compared

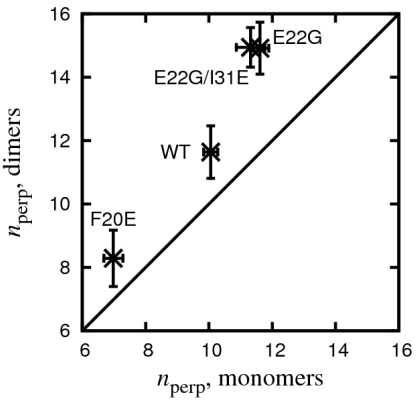

Figure 4: Comparison of n_{perp} for monomers and dimers of the four Aβ42 variants. n_{perp} denotes the average number of intra-chain pair contacts i, j $(i < j)$ within the strip defined by $50 \leq i + j \leq 60$ for a given chain, at T_0.

to WT, we find that n_{perp} is high for E22G and E22G/I31E but low for F20E. Furthermore, a clear trend can be seen for n_{perp} to increase upon dimer formation. The increase is most pronounced for E22G and E22G/I31E.

In addition to the 10–19 hairpin and the turns centered in the 20–30 region, there are also two turns centered at residues 7–10 and 35–38, respectively. These two bands of populated contacts are broad and do not correspond to single β-hairpins, but rather to families of such states. Both these turns are, like the 10–19 hairpin, only weakly affected by the mutations.

So far, we have discussed turn structures populated in our simulations, rather than individual residue pair contact probabilities. A residue pair of special interest is Asp23-Lys28, which forms a salt bridge in both Aβ40 [5] and Aβ42 [6] fibrils. This contact is frequently present in our simulations; the contact probability is at the level of ∼30–40 % for all four Aβ42 variants. The electrostatic Asp23-Lys28 interaction has a turn-stabilizing effect. Turn formation in this part of the Aβ monomer is, according to previous computational studies [24, 25], also driven by hydrophobic interaction between Val24 and the aliphatic part of the Lys28 side chain. Consistent with this, we observe an elevated contact probability for Val24-Lys28 (∼10–15 % for F20E, and ∼15–25 % for WT, E22G and E22G/I31E). A possible difference between Aβ40 and Aβ42 fibrils is in the contacts formed by Phe19, which was found to pack against Leu34 in Aβ40 fibrils [5] but against Gly38 in Aβ42 fibrils [6]. However, the latter result was questioned by a recent study, which observed Phe19-Leu34 packing in both fibrils and oligomers of Aβ42 [9]. In our simulations, the contact probability varies between ∼20–40 % for Phe19-Leu34, depending on Aβ42 variant, the order be-

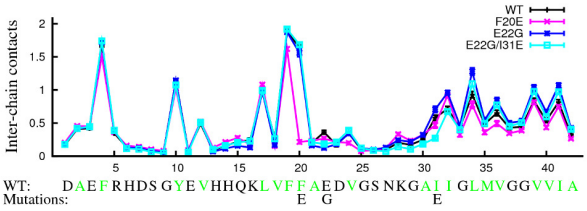

Figure 5: The average number of inter-chain contacts that a given residue is involved in. The WT amino acid sequence and the mutations studied are indicated along the x-axis, with hydrophobic amino acids in green. Data are taken at T_0.

ing F20E<WT<E22G/I31E<E22G. The Phe19-Gly38 contact probability is markedly lower, $\lesssim 7\,\%$, irrespective of Aβ42 variant.

Intermolecular interactions. We now turn from the intra- to the inter-chain contact maps. In the inter-chain case, there is a small group of residues responsible for all strong contacts (Fig. 3). No clear bands of contacts perpendicular or parallel to the diagonal can be seen, which, in particular, shows that intermolecular β-sheets are rare.

Figure 5 displays how the average number of inter-chain contacts that a given residue is involved in varies along the peptides. The shape of these profiles can in part be explained by the distribution of hydrophobic residues. The residues involved in most inter-chain contacts (Phe4, Phe19 and Phe20) are found in the N-terminal half of the peptides, and are all strongly hydrophobic. A majority of residues 1–21 are, by contrast, polar and participate in very few such contacts. In the C-terminal half, the number of inter-chain contacts is low in the mainly polar 22–30 segment, but elevated in the predominantly hydrophobic 31–42 segment. There is thus a definite correlation between the number of inter-chain contacts formed by a residue and its hydrophobicity, which shows that hydrophobic attraction is vital for the stability of the simulated dimers.

Another potentially important stabilizing force is inter-chain H bonding. However, we already noted that intermolecular β-sheets are rare in our simulations, and it turns out that the average total number of inter-chain H bonds formed is low; it varies between 5–7, depending on Aβ42 variant. Inter-chain H bonding, therefore, provides only a limited contribution to the stability of the dimers.

Intermolecular contacts at the onset of aggregation. The above analysis of inter-chain contacts pertains to the temperature T_0, well into the dimer regime. Also interesting is the behavior in the monomer-dimer coexistence region, where the first inter-chain contacts appear. In our simula-

Table 1: Average numbers of inter-chain contacts that the N-terminal (n_N) and C-terminal (n_C) halves of a given peptide are involved in.

	WT		F20E	
	T_0	1.09 T_0	T_0	1.04 T_0
n_N	9.9 ± 0.4	3.1 ± 0.1	8.2 ± 0.1	2.6 ± 0.4
n_C	9.2 ± 1.3	0.9 ± 0.1	7.2 ± 0.3	1.3 ± 0.2

tions, many of these early contacts are between residues belonging to the N-terminal halves of the peptides. To make this precise, let n_N and n_C denote the average total numbers of inter-chain contacts formed by, respectively, the N- and C-terminal halves of a given peptide. Table 1 shows n_N and n_C for WT and F20E, both at monomer-dimer coexistence and at T_0. The data for E22G and E22G/I31E are very similar to the WT data and therefore not shown.

For WT, we find that n_N exceeds n_C by a factor $\sim$3 at the coexistence temperature 1.09 T_0. This asymmetry indicates that the N-terminal half plays a driving role at the onset of aggregation. Note that n_N and n_C, by contrast, are similar at T_0.

The results obtained for F20E are qualitatively similar, but the difference between n_N and n_C in the coexistence region is less pronounced for this variant. The lower degree of asymmetry between the N- and C-terminal halves corroborates the earlier observation that dimer formation is more cooperative for F20E.

Examples of dimer conformations. A large part of our analysis so far has dealt with average values of conformational parameters. To further characterize the simulated dimer ensembles, we apply a clustering procedure, based on a distance function that measures the dissimilarity between two sets of inter-chain contacts (see Methods). Despite the use of a fairly large maximum cluster diameter, all clusters found have populations $< 6\,\%$, for all four Aβ42 variants. The absence of large clusters confirms that the simulated ensembles are conformationally heterogeneous, as suggested by the shape of the free energies in Figs. 1 and 2.

Figure 6 shows the centroids of five clusters for WT, along with the minimum-energy conformation found in the simulations. These five clusters are the ones most frequently visited in the simulations (frequencies between 1–6 %), but there are other clusters whose populations are not significantly lower. The figure illustrates the fact that the observed dimers are topologically diverse.

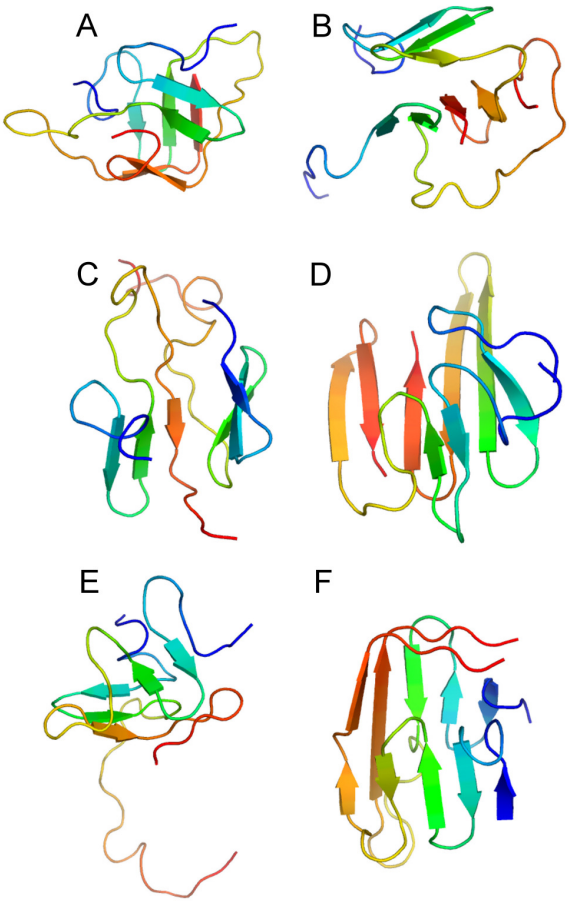

Figure 6: Examples of dimer conformations from our Aβ42 WT simulations. The coloring is such that the N and C termini are blue and red, respectively. (A-E) Cluster centroids illustrating the diversity of the simulated dimer ensemble, from a clustering based on inter-chain contacts, at T_0. The centroids represent the five most frequently visited clusters. The populations are low (1–6 %) and there are other clusters of similar size. (F) The minimum-energy conformation found in the simulations.

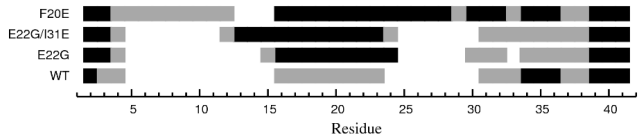

Figure 7: Location of the in-register parallel β-sheets observed in the simulations. White, gray and black indicate frequencies of occurrence of <0.1 %, 0.1–1 %, and >1 %, respectively, at T_0. The frequency is low (<6 %) for all residues in all four Aβ42 variants.

Intermolecular β-sheet structure. As indicated, for instance, by the contact maps, intramolecular antiparallel β-sheets are the by far most common type of secondary structure in our simulations. The β-sheets in Aβ fibrils are intermolecular instead, with an in-register parallel organization of the strands [5, 6]. An example of this type of structure from our simulations can be seen in Fig. 6*F* (red strands).

To estimate the amount and location of in-register parallel β-sheets, we compute the probability for each residue to be involved in H bonds compatible with this type of structure. This probability is low (<6 %) for all residues in all four Aβ42 variants, as expected from the absence of visible bands on the main diagonal of the inter-chain contact maps (Fig. 3).

Figure 7 illustrates the location of the observed in-register parallel β-sheets along the four Aβ42 sequences. Due to statistical uncertainties, a simplified ternary frequency scale is used. Although the frequencies are low, the data for WT, E22G and E22G/I31E show a clear common pattern. In the two regions 5–11 and 25–29 virtually no in-register parallel β-sheets occur for any of these three variants. By contrast, for all three variants, such structure is observed in a small region near the N terminus, around the central hydrophobic core (CHC; residues 17–21), and toward the C terminus. The distribution is more uniform along the chain for F20E.

For WT, E22G and E22G/I31E, we thus observe in-register parallel β-sheets around the CHC and toward the C terminus but very little such structure in the intermediate 25–29 region, a pattern that matches well with the β-loop-β motif in Aβ fibrils [5, 6]. It must be remembered, however, that this type of structure is rare in the simulations, for all four variants.

Discussion

To gain insight into the structure and formation of Aβ dimers, we have performed an extensive MC study of four Aβ42 variants with known and very different aggregation propensities [11, 13].

In terms of overall conformational properties, our results are similar for these Aβ42 variants. In particular, in all four cases, we find that the main type of secondary structure is intramolecular antiparallel β-sheets, and thus different than that in Aβ fibrils. The α-helix content was low in our previous study of the monomers [18], and is even lower for the dimers.

At first glance, our observation of a stable dimer phase may seem to contradict the simulations of Urbanc et al. [14], who analyzed the stability of a set of planar dimer structures using an all-atom model with explicit solvent. They found that these states had higher free energies than the corresponding monomeric states. Our dimer ensembles are diverse and consist predominantly of non-planar structures. Hence, there is no contradiction to the findings of Urbanc et al.

The existence and location of the observed intramolecular antiparallel β-sheets are in broad agreement with recent experimental analyses of Aβ oligomers [8–10]. Detailed NMR-based characterizations were reported for two oligomeric Aβ species, a tetramer [8] and a pentamer [9]. The tetramer, termed preglobulomer, was found to contain intermolecular in-register parallel β-sheets involving residues 34–41 [8], as well as an intramolecular β-hairpin formed by residues 19–32. A similarly centered antiparallel structure is seen our simulation, although it is not a well-defined β-hairpin. Within the pentamer, each Aβ monomer was found to have a compact fold with strands and turns, but no proper β-sheet structure [9]. Three solvent-accessible regions were identified, namely 13–15, 25–29 and 37–38, which virtually coincide with the three main turn regions seen in our simulations (Fig. 3).

Different lines of research indicate that the middle of these three turn regions, near the loop in Aβ fibrils, might play a key role in aggregation. Studies of the Aβ(21–30) fragment found that it adopts a bend structure, favored by both hydrophobic and electrostatic interactions, which is destabilized by several AD-linked mutations in a manner that correlates with Aβ oligomerization propensity [25–27]. It was further demonstrated that the coupling of the Asp23 and Lys28 side chains in Aβ40 through a lactam bridge leads to a much faster fibril formation [28], potentially by increasing the population of assembly competent conformations [29].

In our calculations, we observe conformational changes caused by mutations as well as by dimerization in this part of Aβ42. A clear illustration is the n_{perp} analysis, where n_{perp} is a simple contact-based measure of the propensity for formation of turns centered in the 25–30 region. We find that the four variants have different n_{perp}, and that in all cases the magnitude increases upon dimerization (Fig. 4).

Two frequently occurring intramolecular contacts in our simulations are Asp23-Lys28 and Phe19-Leu34. They have been recognized as key interactions in Aβ fibrils [5, 6, 9], and the latter has also

been found in Aβ40 bound to an Affibody protein [30]. Our analysis suggests that the Phe19-Leu34 contact probability is mutation sensitive. The rank order among the Aβ42 variants with respect to this contact probability as well as to n_{perp} and experimentally measured fibril formation rates [11] is F20E<WT<E22G/I31E$\lesssim$E22G. These observations are consistent with a general picture in which only certain conformational states are aggregation competent, and mutations affect the aggregation propensity by altering the population of these states [29]. In our simulations, fibril-like conformational properties are altered by the mutations, and the observed changes correlate with measured fibril formation rates [11].

In-register parallel β-sheets were observed near the C terminus in the above-mentioned pentamer study [9], but occur in only small amounts in our simulations. We find low populations of such structure around the CHC and toward the C terminus, while it is virtually absent in the two regions 5–11 and 25–29 for WT, E22G and E22G/I31E. This pattern bears a resemblance to the β-loop-β motif in Aβ fibrils, but needs a firmer statistical verification. F20E, on the other hand, has a more uniform distribution of in-register parallel β-sheets along the chain.

The main stabilizing force for the simulated dimers is hydrophobicity, as indicated by a clear correlation between the average number of inter-chain contacts for a given residue and its hydrophobicity. The residues involved in most inter-chain contacts are Phe4, Phe19 and Phe20, the latter two of which belong to the CHC. Our calculations are, therefore, consistent with a driving role for the CHC in Aβ aggregation [31]. In line with this hypothesis is the observation of a reduced aggregation propensity for F20E, in experiments [11] as well as in our simulations.

Among the WT, E22G and E22G/I31E variants, we observe only minor dissimilarities in dimerization propensity, while it is known that there are marked differences in their predisposition for forming larger aggregates [11]. A possible explanation is that the aggregates must be structurally more regular and uniform in order for mutation-induced conformational changes to play a role. A clear tendency toward more regular and uniform aggregates with increasing aggregate size was recently observed in simulations with up to 32 chains for a small fibril-forming peptide [32]. Therefore, it is, despite the challenge, of utmost interest to pursue the simulations of Aβ aggregation to larger systems. Already at the dimer level, we observe conformational features not easily anticipated from monomer studies.

Methods

We study Aβ42 dimerization using all-atom MC simulations with implicit solvent. The potential we use is composed of four terms, $E = E_{\rm loc} + E_{\rm ev} + E_{\rm hb} + E_{\rm sc}$. The first term, $E_{\rm loc}$, contains local interactions between atoms separated by only a few covalent bonds. The other three terms are nonlocal in character: $E_{\rm ev}$ represents excluded-volume effects, $E_{\rm hb}$ is a hydrogen-bond potential, and $E_{\rm sc}$ describes residue-specific interactions, based on hydrophobicity and charge, between pairs of side chains. A full description of the potential can be found elsewhere [17].

Our use of implicit solvent represents a coarse-graining in the description of the systems, and means that some potentially important questions cannot be addressed. For example, we cannot clearly distinguish between solvated and proper salt bridges [33], or study the effects of discrete water molecules on fibrils [34] or fibril formation [35]. Such effects are only included in a mean-field sense in our calculations. The advantage of using implicit solvent is that it makes it possible for us to study the interaction of two unconstrained full-length Aβ molecules, which otherwise would be out of reach on today's computers.

The possibilities to directly relate our dimer simulations to existing computational or experimental studies are limited. However, our previous monomer simulations [18] can be compared, e.g., with the combined molecular dynamics and NMR study of Sgourakis et al. [36,37]. Our results were similar to theirs with respect to turn locations. However, the β-strand content was higher in our simulations than it was in theirs, and than what has been been found by deconvolution of circular dichroism measurements [38]. This could indicate that our force field overestimates the strand content. Therefore, to test our methods, we calculated J-couplings and chemical shifts, which depend on secondary structure and can be estimated from simulations in a relatively direct manner. Our calculated J-couplings were compared with the experimental values obtained by Sgourakis et al. [36], with good results [18]. In particular, no sign was found that the strand content was overestimated in our simulations. Our calculated chemical shifts were compared with the experimental data of Hou et al. [20], with the same conclusion [18].

In the present article, we simulate the equilibrium properties of systems of two Aβ42 peptides enclosed in a periodic box of size $(200\,\text{Å})^3$. The simulations are started from random initial conformations and carried out using simulated tempering [39, 40] with five temperatures, ranging from T_0 to $\sim$1.2 T_0. The simulation temperature T_0 corresponds to $\sim$273–278 K, based on comparisons of our Aβ42 WT monomer simulations with NMR measurements [18]. The elementary moves employed are rotations of individual backbone and side-chain angles, concerted rotations of sets of

eight backbone angles [41], and rigid-body translations and rotations of whole chains.

For each of the Aβ42 variants studied (WT, F20E, E22G, E22G/I31E), we perform 40 independent runs, using the open source C++-package PROFASI [42]. Each run comprises $2 \cdot 10^{10}$ MC steps, corresponding to ~ 60 CPU days on a 3 GHz Intel Xeon 5160 core. The first 10 % of each run is discarded for thermalization. Mean values and statistical errors are calculated by using the jackknife method [43].

In our analysis of the simulations, secondary structure assignments are determined by using the STRIDE program [44]. The center-of-mass distance between the two peptides, D_{cm}, and the radius of gyration of a chain, R_{g}, are computed over all non-hydrogen atoms. A contact between two residues which are not nearest or next-nearest neighbors along the chain, is defined as follows. A pair of heavy atoms closer than 4.5 Å, one from each residue, is said to provide a link between the residues. Residue pairs with two or more links are defined to be in contact.

The generated conformations are clustered based on which inter-chain contacts they contain, by using the QT algorithm [45]. As maximum cluster diameter a Jaccard distance of 0.667 is used, where the Jaccard distance between two sets A and B is given by $1 - |A \cap B|/|A \cup B|$.

Figures of 3D structures are prepared using PyMOL [46].

Acknowledgements

We thank Dr. Sandipan Mohanty for assistance with the calculations. The simulations were performed at the LUNARC facility in Lund. This work was in part funded by the Swedish Research Council.

References

[1] D. M. Walsh, D. J. Selkoe, Aβ oligomers – a decade of discovery, J. Neurochem. 101 (2007) 1172–1184.

[2] G. M. Shankar, S. Li, T. H. Mehta, A. Garcia-Munoz, N. E. Shepardson, I. Smith, M. A. Brett, Francesca M AU Farrell, M. J. Rowan, C. A. Lemere, C. M. Regan, D. M. Walsh, B. L. Sabatini, D. J. Selkoe, Amyloid-β protein dimers isolated directly from Alzheimer's brains impair synaptic plasticity and memory, Nat. Med. 14 (2008) 837–842.

[3] T. Tomiyama, T. Nagata, H. Shimada, R. Teraoka, A. Fukushima, H. Kanemitsu, H. Takuma, R. Kuwano, M. Imagawa, S. Ataka, Y. Wada, E. Yoshioka, T. Nishizaki, Y. Watanabe, H. Mori, A new amyloid β variant favoring oligomerization in Alzheimer's-type dementia, Ann. Neurol. 63 (2008) 377–387.

[4] A. Sandberg, L. M. Luheshi, S. Söllvander, T. P. D. Barros, B. Macao, T. P. J. Knowles, H. B. l, C. Lendel, F. Ekholm-Petterson, A. Dubnovitsky, L. Lannfelt, C. M. Dobson, T. Härd, Stabilization of neurotoxic Alzheimer amyloid-β oligomers by protein engineering, Proc. Natl. Acad. Sci. USA 107 (2010) 15595–15600.

[5] A. T. Petkova, Y. Ishii, J. J. Balbach, O. N. Antzutkin, R. D. Leapman, F. Delaglio, R. Tycko, A structural model for Alzheimer's β-amyloid fibrils based on experimental constraints from solid state NMR, Proc. Natl. Acad. Sci. USA 99 (2002) 16742–16747.

[6] T. Lührs, C. Ritter, M. Adrian, D. Riek-Loher, B. Bohrmann, H. Döbeli, D. Schubert, R. Riek, 3D structure of Alzheimer's amyloid-β(1-42) fibrils, Proc. Natl. Acad. Sci. USA 102 (2005) 17342–17347.

[7] R. Tycko, K. L. Sciarretta, J. P. R. O. Orgel, S. C. Meredith, Evidence for novel β-sheet structures in Iowa mutant β-amyloid fibrils, Biochemistry 48 (2009) 6072–6084.

[8] L. Yu, R. Edalji, J. E. Harlan, T. F. Holzman, A. P. Lopez, B. Labkovsky, H. Hillen, S. Barghorn, U. Ebert, P. L. Richardson, L. Miesbauer, L. Solomon, D. Bartley, K. Walter, R. W. Johnson, P. J. Hajduk, E. T. Olejniczak, Structural characterization of a soluble amyloid β-peptide oligomer, Biochemistry 48 (2009) 1870–1877.

[9] M. Ahmed, J. Davis, D. Aucoin, T. Sato, S. Ahuja, S. Aimoto, J. I. Elliott, W. E. V. Nostrand, S. O. Smith, Structural conversion of neurotoxic amyloid-β_{1-42} oligomers to fibrils, Nat. Struct. Mol. Biol. 17 (2010) 561–567.

[10] E. Cerf, R. Sarroukh, S. Tamamizu-Kato, L. Breydo, S. Derclaye, Y. F. Dufrêne, V. Narayanaswami, E. Goormaghtigh, J.-M. Ruysschaert, V. Raussens, Antiparallel β-sheet: a signature structure of the oligomeric amyloid β-peptide, Biochem. J. 421 (2009) 415–423.

[11] L. M. Luheshi, G. G. Tartaglia, A. Brorsson, A. P. Pawar, I. E. Watson, F. Chiti, M. Vendruscolo, D. A. Lomas, C. M. Dobson, D. C. Crowther, Systematic in vivo analysis of the intrinsic determinants of amyloid β pathogenicity, PLoS Biol. 5 (2007) e290.

[12] C. Nilsberth, A. Westlind-Danielsson, C. B. Eckman, M. M. Condron, K. Axelman, C. Forsell, C. Stenh, J. Luthman, D. B. Teplow, S. G. Younkin, J. Näslund, L. Lannfelt, The 'Arctic' APP mutation (E693G) causes Alzheimer's disease by enhanced Aβ protofibril formation, Nat. Neurosci. 4 (2001) 887–893.

[13] A.-C. Brorsson, B. Bolognesi, G. G. Tartaglia, S. L. Shammas, G. Favrin, I. Watson, D. A. Lomas, F. Chiti, M. Vendruscolo, C. M. Dobson, D. C. Crowther, L. M. Luheshi, Intrinsic determinants of neurotoxic aggregate formation by the amyloid β peptide, Biophys. J. 98 (2010) 1677–1684.

[14] B. Urbanc, L. Cruz, F. Ding, D. Sammond, S. Khare, S. V. Buldyrev, H. E. Stanley, N. V. Dokholyan, Molecular dynamics simulation of amyloid beta dimer formation, Biophys. J. 87 (2004) 2310–2321.

[15] A. Melquiond, X. Dong, N. Mousseau, P. Derreumaux, Role of the region 23–28 in Aβ fibril formation: insights from simulations of the monomers and dimers of Alzheimer's peptides Aβ40 and Aβ42, Curr. Alzheimer Res. 5 (2009) 244–250.

[16] P. Anand, F. S. Nandel, U. H. E. Hansmann, The Alzheimer β-amyloid (Aβ_{1-39}) dimer in an implicit solvent, J. Chem. Phys. 21 (2008) 195102.

[17] A. Irbäck, S. Mitternacht, S. Mohanty, An effective all-atom potential for proteins, PMC Biophys. 2 (2009) 2.

[18] S. Mitternacht, I. Staneva, T. Härd, A. Irbäck, Comparing the folding free-energy landscapes of Aβ42 variants with different aggregation properties, Proteins 78 (2010) 2600–2608.

[19] R. Riek, P. Güntert, H. Döbeli, B. Wipf, K. Wüthrich, NMR studies in aqueous solution fail to identify significant conformational differences between the monomeric forms of two Alzheimer peptides with widely different plaque-competence, Aβ40^{ox} and Aβ42^{ox}, Eur. J. Biochem. 268 (2001) 5930–5936.

[20] L. Hou, H. Shao, Y. Zhang, H. Li, N. K. Menon, E. B. Neuhaus, J. M. Brewer, I. J. L. Byeon, D. G. Ray, M. P. Vitek, T. Iwashita, R. A. Makula, A. B. Przybyla, M. G. Zagorski, Solution NMR studies of the Aβ40 and Aβ42 peptides establish that the Met35 oxidation state affects the mechanism of amyloid formation, J. Am. Chem. Soc. 126 (2004) 1992–2005.

[21] Y. Yan, C. Wang, Aβ42 is more rigid than Aβ40 at the C terminus: implications for Aβ aggregation and toxicity, J. Mol. Biol. 364 (2006) 853–862.

[22] A. Olofsson, A. E. Sauer-Eriksson, A. Öhman, The solvent protection of Alzheimer amyloid-β-(1–42) fibrils as determined by solution NMR spectroscopy, J. Biol. Chem. 281 (2006) 477–483.

[23] Y. Masuda, S. Uemura, R. Ohashi, A. Nakanishi, K. Takegoshi, T. Shimizu, T. Shirasawa, K. Irie, Identification of physiological and toxic conformations in Aβ aggregates, ChemBioChem 10 (2009) 287–295.

[24] J. M. Borreguero, B. Urbanc, N. D. Lazo, S. V. Buldyrev, D. B. Teplow, H. E. Stanley, Folding events in the 21-30 region of amyloid β-protein (Aβ) studied in silico, Proc. Natl. Acad. Sci. USA 102 (2005) 6015–6020.

[25] B. Tarus, J. E. Straub, D. Thirumalai, Structures and free-energy landscapes of the wild type and mutants of the Aβ(21-30) peptide are determined by an interplay between intrapeptide electrostatic and hydrophobic interactions, J. Mol. Biol. 379 (2008) 815–829.

[26] M. A. Grant, N. D. Lazo, A. Lomakin, M. M. Condron, H. Arai, G. Yamin, A. C. Rigby, D. B. Teplow, Familial Alzheimer's disease mutations alter the stability of the amyloid β-protein monomer folding nucleus, Proc. Natl. Acad. Sci. USA 104 (2007) 16522–16527.

[27] M. M. Murray, M. G. Krone, S. L. Bernstein, A. Baumketner, M. M. Condron, N. D. Lazo, D. B. Teplow, T. Wyttenbach, J.-E. Shea, M. T. Bowers, Amyloid β-protein: experiment and theory on the 21-30 fragment, J. Phys. Chem. B 113 (2009) 6041–6046.

[28] K. L. Sciarretta, D. J. Gordon, A. T. Petkova, R. Tycko, S. C. Meredith, Aβ40-Lactam(D23/K28) models a conformation highly favorable for nucleation of amyloid, Biochemistry 44 (2005) 6003–6014.

[29] G. Reddy, J. E. Straub, D. Thirumalai, Influence of preformed Asp23-Lys28 salt bridge on the conformational fluctuations of monomers and dimers of Aβ peptides with implications for rates of fibril formation, J Phys Chem B 113 (2009) 1162–1172.

[30] W. Hoyer, C. Grönwall, A. Jonsson, S. Ståhl, T. Härd, Stabilization of a β-hairpin in monomeric Alzheimer's amyloid-β peptide inhibits amyloid formation, Proc. Natl. Acad. Sci. USA 105 (2008) 5099–5104.

[31] L. O. Tjernberg, J. Näslund, F. Lindqvist, J. Johansson, A. R. Karlström, J. Thyberg, L. Terenius, C. Nordstedt, Arrest of β-amyloid fibril formation by pentapeptide ligand, J. Biol. Chem. 271 (1996) 8545–8548.

[32] D. Li, S. Mohanty, A. Irbäck, S. Huo, Formation and growth of oligomers: a Monte Carlo study of an amyloid tau fragment, PLoS Comput. Biol. 4 (2008) e1000238.

[33] B. Tarus, J. E. Straub, D. Thirumalai, Dynamics of Asp23-Lys28 salt-bridge formation in Aβ_{10-35} monomers, J. Am. Chem. Soc. 128 (2006) 16159–16168.

[34] Y. S. Kim, L. Liu, P. H. Axelsen, R. M. Hochstrasser, 2D IR provides evidence for mobile water molecules in β-amyloid fibrils, Proc. Natl. Acad. Sci. USA 106 (2009) 17751–17756.

[35] G. Reddy, J. E. Straub, D. Thirumalai, Dynamics of locking of peptides onto growing amyloid fibrils, Proc. Natl. Acad. Sci. USA 106 (2009) 11948–11953.

[36] N. G. Sgourakis, Y. Yan, S. A. McCallum, C. Wang, A. E. García, The Alzheimer's peptides Aβ40 and 42 adopt distinct conformations in water: a combined MD/NMR study, J. Mol. Biol. 368 (2007) 1448–1457.

[37] N. G. Sgourakis, M. Merced-Serrano, C. Boutsidis, P. Drineas, Z. Du, C. Wang, A. E. García, Atomic-level characterization of the ensemble of the aβ(1–42) monomer in water using unbiased molecular dynamics simulations and spectral algorithms, J. Mol. Biol. 405 (2011) 570–583.

[38] M. D. Kirkitadze, M. M. Condron, D. B. Teplow, Identification and characterization of key kinetic intermediates in amyloid β-protein fibrillogenesis, J. Mol. Biol. 312 (2001) 1103–1119.

[39] A. P. Lyubartsev, A. A. Martsinovski, S. V. Shevkunov, P. N. Vorontsov-Velyaminov, New approach to Monte Carlo calculation of the free energy: method of expanded ensembles, J. Chem. Phys. 96 (1992) 1776–1783.

[40] E. Marinari, G. Parisi, Simulated tempering: a new Monte Carlo scheme, Europhys. Lett. 19 (1992) 451–458.

[41] G. Favrin, A. Irbäck, F. Sjunnesson, Monte Carlo update for chain molecules: Biased Gaussian steps in torsional space, J. Chem. Phys. 114 (2001) 8154–8158.

[42] A. Irbäck, S. Mohanty, PROFASI: a Monte Carlo simulation package for protein folding and aggregation, J. Comput. Chem. 27 (2006) 1548–1555.

[43] R. G. Miller, The jackknife – a review, Biometrika 61 (1974) 1–15.

[44] D. Frishman, P. Argos, Knowledge-based protein secondary structure assignment, Proteins 23 (1995) 566–579.

[45] L. J. Heyer, S. Kruglyak, S. Yooseph, Exploring expression data: identification and analysis of coexpressed genes, Genome Res. 9 (1999) 1106–1115.

[46] W. L. DeLano, The PyMOL molecular graphics system, San Carlos, CA: DeLano Scientific (2002).